Composites: Part B 43 (2012) 2594–2604

Contents lists available at SciVerse ScienceDirect

Composites: Part B

journal homepage: www.elsevier.com/locate/compositesb

Material parameters for pressure-dependent yielding of unidirectional fiber-reinforced polymeric composites

R.C. Batra [a,*], G. Gopinath [a], J.Q. Zheng [b]

[a] Department of Engineering Science and Mechanics, Virginia Polytechnic Institute and State University, Blacksburg, VA 24061, USA
[b] Program Executive Office – Soldier, US Army, 15395 John Marshall Highway, Haymarket, VA 20169, USA

ARTICLE INFO

Article history:
Received 16 October 2011
Received in revised form 28 November 2011
Accepted 19 December 2011
Available online 30 December 2011

Keywords:
A. Polymer–matrix composites (PMCs)
B. Plastic deformation
C. Micromechanics
Homogenization

ABSTRACT

We study elasto-plastic deformations of unidirectional fiber reinforced polymeric composites (UFPCs) with fibers assumed to deform elastically and the matrix elasto-plastically. The matrix's and hence composite's plastic deformations are analyzed by using both the pressure-independent von Mises yield surface and the pressure-dependent Drucker–Prager yield surface and the associated flow rules. In both cases the strain hardening of the matrix is considered and values of material parameters for the matrix are obtained by computing the effective stress versus the effective plastic strain curves from experimental uniaxial stress–strain curves. Values of parameters in the yield surface for the UFPC in terms of those of the matrix and the volume fraction of fibers are found by using a micromechanics approach. Wherever possible, the computed results are compared with the corresponding experimental findings available in the literature. Significant contributions of the work include providing a methodology for determining values of elasto-plastic material parameters for a UFPC from those of its constituents and their volume fractions, and giving expressions in terms of volume fractions of fibers for material parameters appearing in the yield surface of the composite.

1. Introduction

Composites being inhomogeneous materials provide challenges in design since their failure mechanisms are not well understood. Furthermore, for design purposes, one needs to find properties of a homogeneous material equivalent in mechanical response to the composite. Several homogenization techniques have been proposed in the literature to find mechanical properties of the composite from those of its constituents when deformations are linear elastic; for example, see books by Torquato [1], Suquet [2], Bensoussan et al. [3], Nemat-Nasser and Hori [4], Mura [5], Aboudi [6,18], Tsai and Hahn [7], Hyer [8], and Reifsnider and Case [9], and the review paper by Charalambakis [10]. In contrast to the micromechanical theories, Love and Batra [11] numerically simulated plane strain elasto-plastic deformations of a metal matrix composite with circular cylindrical fibers, by keeping edges of the cross-section plane and deduced values of the elastic and the plastic parameters at different strains and strain rates by assuming that under quasistatic deformations the initial yield stress of the composite is given by the rule of mixtures.

We note that, in general, Young's modulus of a lamina in the direction of fibers is considerably more than that in directions orthogonal to fibers. Most fibers undergo infinitesimal elastic deformations prior to failure, but the matrix bonding the fibers can deform in-elastically. Hence it can be assumed that inelastic deformation in the composite is due to that of the matrix.

Bridgman [12] experimentally showed that the hydrostatic pressure does not affect plastic deformations of metals. However, mechanical deformations of some polymers have been shown to be influenced by the hydrostatic pressure. Thus the yield surface for such a polymer should depend upon the hydrostatic pressure; this dependence has been considered, among others, by Caddell et al. [13], and Hu and Pae [14]. The reader is referred to the World Wide Exercise paper [30] summarizing activities in this aspect of the problem. Here we consider two such yield criteria for the matrix and account for matrix's strain hardening. The yield surfaces for unidirectional fiber reinforced polymeric composites (UFPCs) are deduced by making the following assumptions: (i) the UFPC is a transversely isotropic material with the fiber axis as the axis of transverse isotropy, (ii) there is no plastic deformation in the direction of fibers, (iii) fibers deform elastically, (iv) fibers are perfectly bonded to the matrix, (v) fibers are transversely isotropic with fiber axis as the axis of transverse isotropy, and (vi) the matrix is isotropic and obeys either the

* Corresponding author.
E-mail address: rbatra@vt.edu (R.C. Batra).

1359-8368/$ - see front matter © 2011 Elsevier Ltd. All rights reserved.
doi:10.1016/j.compositesb.2011.12.005

Drucker–Prager pressure dependent yield criterion or the pressure independent von Mises yield criterion. We use a micromechanical theory based on the method of cells called free shear traction (FST) method [15] to quantify the dependence of values of material parameters appearing in the yield surface as a function of the volume fraction of fibers and mechanical properties of the matrix and the fibers. The use of homogenized material parameters is very useful as it offers an efficient way of analyzing deformations of composite structures. However, it smears out singularities in stresses and deformations at interfaces between dissimilar materials, and thus may underestimate damage and failure initiation and propagation. The functional dependence of the effective stress of the composite upon the effective plastic strain (i.e., the strain hardening effect) is taken to be similar to that of the matrix. This paper generalizes Weeks and Sun's [26] work to pressure-dependent yielding of polymers often observed in experiments, and provides a different technique for finding values of material parameters.

The rest of the paper is organized as follows. Section 2 describes pressure-dependent and pressure-independent yield surfaces for the matrix and the UFPC, and techniques to evaluate various material parameters appearing in the yield surface of the UFPC. For an AS4/PEEK composite, the computed numerical results are compared with the experimental findings available in the literature in Section 3, and conclusions of this study are summarized in Section 4 where values of material parameters in the yield surface for the UFPC as a function of the volume fraction of fibers are given. In the appendix we have briefly reviewed the FST approach and have also compared results obtained by this method with those computed using the Mori–Tanaka (M–T) scheme. The FST scheme is computationally less expensive than the M–T method and provides reasonably good values of material parameters. In the M–T scheme, when the matrix deforms plastically an iterative process is used to determine the Eshelby tensor because the elasto-plastic properties of the matrix are unknown a priori. Numerically finding the Eshelby tensors needed to compute the concentration tensor (e.g., see [17,33–35]) in an elasto-plastic problem is computationally more expensive than solving a small system of algebraic equations in the FST method.

2. Elasto-plastic material parameters

2.1. Preliminaries

The polymer in a UFPC usually exhibits an elasto-plastic response. However fibers deform elastically and exhibit brittle failure. Consequently, the failure strain of a UFPC in the direction of fibers is small. Furthermore, deformations transverse to fibers prior to failure are also infinitesimal and one can neglect effects of geometric nonlinearities. We first briefly review elasto-plastic deformations of the polymer and the UFPC and then use a micromechanics approach [15] to determine parameters appearing in the plastic potential and the functional dependence of the effective stress on the effective plastic strain of a UFPC.

2.2. Infinitesimal elasto-plastic deformations of polymer

2.2.1. Pressure independent yielding of polymer

We employ incremental theory of plasticity and assume that during infinitesimal deformations, the increment, $d\boldsymbol{e}$, in strains has an additive decomposition into elastic, $d\boldsymbol{e}^e$, and plastic, $d\boldsymbol{e}^p$, strains, i.e.,

$$d\boldsymbol{e} = d\boldsymbol{e}^e + d\boldsymbol{e}^p \tag{2.1}$$

For relating $d\boldsymbol{e}^p$ to $d\boldsymbol{\sigma}$, we assume the von Mises plastic potential [19] for the polymer, i.e.,

$$2F(\sigma_{ij}) = \frac{1}{3}(\sigma_{22}-\sigma_{33})^2 + \frac{1}{3}(\sigma_{33}-\sigma_{11})^2 + \frac{1}{3}(\sigma_{11}-\sigma_{22})^2 + 2\sigma_{23}^2 + 2\sigma_{31}^2 + 2\sigma_{12}^2 \tag{2.2}$$

Here we have used rectangular Cartesian coordinates, and have expressed the plastic potential in terms of the stress tensor $\boldsymbol{\sigma}$ rather than in terms of the deviatoric stress $s_{ij} = \sigma_{ij} - \frac{1}{3}\sigma_{kk}\delta_{ij}$. In Eq. (2.2) we have tacitly assumed that the polymer is an isotropic material.

We use the associated flow rule for relating $d\boldsymbol{e}^p$ to $d\boldsymbol{\sigma}$, i.e.,

$$de_{ij}^p = d\lambda \frac{\partial F}{\partial \sigma_{ij}} \tag{2.3}$$

where $d\lambda$ is the proportionality factor. Eq. (2.3) implies that $d\boldsymbol{e}^p$ is normal to the yield surface

$$\sqrt{F(\sigma_{ij})} = \sigma^m \tag{2.4}$$

where $\sqrt{3}\sigma^m$ is the yield stress of the polymer in a simple tension or compression test.

We define the effective stress $\bar{\sigma}$ as:

$$\bar{\sigma} = \sqrt{3F(\sigma_{ij})} \tag{2.5}$$

and the effective plastic strain, $\bar{e}^p$, by requiring that in any incremental deformation,

$$de_{ij}^p \sigma_{ij} = \bar{\sigma} d\bar{e}^p \tag{2.6}$$

We note that $\bar{\sigma} = \sigma^m$ in a uniaxial tension or compression test. Substituting for de_{ij}^p in Eq. (2.6) from Eq. (2.3) and using Eq. (2.5) we get,

$$d\lambda = \frac{3}{2}\frac{d\bar{e}^p}{\bar{\sigma}} = \frac{3}{2H^m}\frac{d\bar{\sigma}}{\bar{\sigma}} \tag{2.7}$$

where the strain-hardening modulus, $H^m = \frac{d\bar{\sigma}}{d\bar{e}^p}$, has been assumed to be positive. The function $H^m(\bar{e}^p)$ is found from experimental data.

Taking the differential of both sides of Eq. (2.5) we get,

$$d\bar{\sigma} = \frac{3}{2\bar{\sigma}}\left(\sigma_{ij} - \frac{\sigma_{kk}}{3}\delta_{ij}\right)d\sigma_{ij} \tag{2.8}$$

Substituting for $d\lambda$ from Eq. (2.7) and for $d\bar{\sigma}$ from Eq. (2.8) into Eq. (2.3) we get,

$$de_{ij}^p = \left(\frac{9}{4H^m\bar{\sigma}^2}\right)\left(\sigma_{ij} - \frac{\sigma_{kk}}{3}\delta_{ij}\right)\left(\sigma_{pq} - \frac{\sigma_{ll}}{3}\delta_{pq}\right)d\sigma_{pq} = S_{ijkl}^{mp} d\sigma_{kl} \tag{2.9}$$

where $\boldsymbol{S}^{mp}$ is the plastic compliance matrix of the polymer.

Expressing strain increments on the right-hand side of Eq. (2.1) in terms of incremental stresses we get,

$$d\boldsymbol{e} = \boldsymbol{S}^{me} d\boldsymbol{\sigma} + \boldsymbol{S}^{mp} d\boldsymbol{\sigma} \tag{2.10}$$

where $\boldsymbol{S}^{\mathrm{me}} = (\boldsymbol{C}^m)^{-1}$ is the elastic compliance matrix for the polymer. Hence

$$d\boldsymbol{\sigma} = (\boldsymbol{S}^{me} + \boldsymbol{S}^{mp})^{-1} d\boldsymbol{e} \tag{2.11}$$

which expresses incremental stresses in terms of incremental strains. We note that $\boldsymbol{S}^{mp}$ depends upon current values of $\boldsymbol{\sigma}$, and normal stresses may affect ensuing shear strains.

The dependence of the flow stress, σ^m, in Eq. (2.4) upon the effective plastic strain, $\bar{e}^p$, is determined from the test data. It will also determine H^m.

2.2.2. Pressure-dependent yielding of polymer

To account for the pressure sensitive yielding of polymers, the Drucker–Prager yield potential is used, and the effective stress is taken to be:

$$\bar{\sigma} = \sqrt{3F} + \alpha^m \sigma_{kk} \tag{2.12a}$$

where the parameter α^m accounts for hydrostatic pressure effects. The Drucker–Prager yield surface is given by:

$$\sqrt{3\bar{F}} + \alpha^m \sigma_{kk} = \beta^m \tag{2.12b}$$

where β^m is a material parameter.

Values of parameters α^m and β^m can be found from the magnitudes of the yield stresses σ_y^t and σ_y^c in simple tension and compression tests, respectively, i.e.,

$$\sigma_y^t + \alpha^m \sigma_y^t = \sigma_y^c - \alpha^m \sigma_y^c = \beta^m \tag{2.12c}$$

By following the procedure used to derive Eqs. (2.8) and (2.9) one can deduce an expression for $\boldsymbol{S}^{mp}$ for the Drucker–Prager yield criterion (2.12b)

2.3. Yield function for unidirectional fiber reinforced polymeric composite (UFPC)

2.3.1. Pressure independent yielding of composite

We recall that the axial Young's modulus of reinforcing circular cylindrical fibers is several times higher than that of the polymeric matrix. As for the matrix discussed in Section 2.2, we use the associative flow rule to analyze infinitesimal elastoplastic deformations of a UFPC. We assume that the response of the UFPC is transversely isotropic with the fiber axis as the axis of transverse isotropy, and there is no plastic deformation along the fiber axis since fibers exhibit brittle linear elastic response, i.e.,

$$de_{11}^p = 0 \text{ or } e_{11}^p = 0 \tag{2.13}$$

Following Spencer [20] we write the plastic potential, $\bar{F}$, for a transversely isotropic UFPC as:

$$\bar{F}(\sigma_{ij}) = \frac{1}{2}\left[(\sigma_{22}-\sigma_{33})^2 + 2A_{23}\sigma_{23}^2 + 2A_{12}\left(\sigma_{13}^2+\sigma_{12}^2\right)\right] \tag{2.14}$$

where values of parameters A_{12} and A_{23} depend upon the constituents of the UFPC and their volume fractions. The yield surface for the UFPC is taken to be

$$\sqrt{3\bar{F}} = \bar{\sigma} \tag{2.15}$$

where $\bar{\sigma}$ equals $\sqrt{1.5}\,\sigma_{22}^{yield}$ in uniaxial tensile or compressive loading along the x_2-axis (i.e., transverse to fibers). We follow the same procedure as that used to derive Eq. (2.9) and get

$$[S^p] = \frac{9}{4H^p\bar{\sigma}^2}\begin{bmatrix} 0 & 0 & 0 & 0 & 0 & 0 \\ 0 & (\sigma_{22}-\sigma_{33})^2 & (\sigma_{33}-\sigma_{22})(\sigma_{22}-\sigma_{33}) & 2A_{23}\sigma_{23}(\sigma_{22}-\sigma_{33}) & 2A_{12}\sigma_{13}(\sigma_{22}-\sigma_{33}) & 2A_{12}\sigma_{12}(\sigma_{22}-\sigma_{33}) \\ 0 & (\sigma_{33}-\sigma_{22})(\sigma_{22}-\sigma_{33}) & (\sigma_{33}-\sigma_{22})^2 & 2A_{23}\sigma_{23}(\sigma_{33}-\sigma_{22}) & 2A_{12}\sigma_{13}(\sigma_{33}-\sigma_{22}) & 2A_{12}\sigma_{12}(\sigma_{33}-\sigma_{22}) \\ 0 & 4\sigma_{23}(\sigma_{22}-\sigma_{33}) & 4\sigma_{23}(\sigma_{33}-\sigma_{22}) & (2A_{23}\sigma_{23})^2 & 4A_{23}A_{12}\sigma_{23}\sigma_{13} & 4A_{23}A_{12}\sigma_{23}\sigma_{12} \\ 0 & 2A_{12}\sigma_{13}(\sigma_{22}-\sigma_{33}) & 2A_{12}\sigma_{13}(\sigma_{33}-\sigma_{22}) & 4A_{23}A_{12}\sigma_{23}\sigma_{13} & (2A_{12}\sigma_{13})^2 & (2A_{12})^2\sigma_{13}\sigma_{12} \\ 0 & 2A_{12}\sigma_{12}(\sigma_{22}-\sigma_{33}) & 2A_{12}\sigma_{12}(\sigma_{33}-\sigma_{22}) & 4A_{23}A_{12}\sigma_{23}\sigma_{12} & (2A_{12})^2\sigma_{13}\sigma_{12} & (2A_{12}\sigma_{12})^2 \end{bmatrix}$$

$$\{de^p\} = [S^p]\{d\sigma\} \tag{2.16}$$

where H^p equals the strain hardening modulus of the UFPC, and the stress and the strain increments are written in the Voigt notation.

Knowing the elastic compliance matrix, $\boldsymbol{S}$, for the composite we can determine the elastic–plastic compliance matrix, $(\boldsymbol{S}+\boldsymbol{S}^p)$, of the composite.

2.3.2. Pressure dependent yielding of composite

To account for the pressure sensitive yielding of composites, the Drucker–Prager yield potential for the composite is adopted, and the effective stress is defined as:

$$\bar{\sigma} = \sqrt{3\bar{F}} + \alpha(\sigma_{22}+\sigma_{33}) \tag{2.17}$$

where the parameter α accounts for effects of the hydrostatic pressure on the yielding of the UFPC. The term $\alpha\,(\sigma_{22}+\sigma_{33})$ in Eq. (2.17) does not containσ_{11}because of the assumption $e_{11}^p = 0$ for the UFPC. One can derive the elastic–plastic compliance matrix for this case by following the same procedure as that outlined in Section 2.3.1.

We note that Chen and Sun [31] assumed the composite to be an orthotropic material and its plastic potential to be independent of the dilatational deformation. Furthermore, Cho et al. [32] used a similar plastic potential in the context of the Drucker–Prager plasticity.

2.4. Determination of elastic–plastic parameters of the UFPC

2.4.1. Pressure-independent yield surface

We use the FST [15] method to compute the effective stress versus the effective plastic strain curve for the UFPC from a knowledge of the material properties of the constituents of the UFPC and the volume fraction of fibers. One way to obtain this curve is to study plane stress deformations of a thin lamina with the fiber axis making an angle θ counter clockwise with the loading (i.e., $x-$) axis as shown in Fig. 1. Thus with respect to the global rectangular Cartesian coordinate axes (x, y, z), the only non-zero component of the stress tensor is σ_{xx}.

Using either the Mohr circle or the stress transformation equations, stresses with respect to the material principal axes (x_1, x_2, x_3) are given by:

$$\sigma_{11} = \sigma_{xx}cos^2\theta,\ \sigma_{22} = \sigma_{xx}sin^2\theta \text{ and } \sigma_{12} = -\sigma_{xx}sin\theta cos\theta \tag{2.18}$$

Substituting for stresses from Eq. (2.18) into Eq. (2.14), and the result into Eq. (2.15) we get

$$\bar{\sigma} = \sqrt{\frac{3}{2}}[sin^4\theta + 2A_{12}sin^2\theta cos^2\theta]^{1/2}\sigma_{xx} \tag{2.19}$$

It follows from Eq. (2.6) that

$$\bar{\sigma}d\bar{e}^p = de_{xx}^p\sigma_{xx} \tag{2.20}$$

and therefore

$$d\bar{e}^p = \frac{de_{xx}^p}{\sqrt{\frac{3}{2}}[sin^4\theta + 2A_{12}sin^2\theta cos^2\theta]^{1/2}} \tag{2.21}$$

Thus

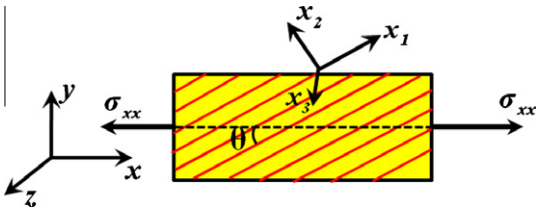

Fig. 1. Fiber orientation with respect to the axis of loading, and the material principal axes (x_1, x_2, x_3).

$$\bar{e}^p = \frac{e_{xx} - \sigma_{xx}/E_{xx}}{\sqrt{\frac{2}{3}}[sin^4\theta + 2A_{12}sin^2\theta cos^2\theta]^{1/2}} \tag{2.22}$$

Here E_{xx} is Young's modulus in the x-direction and it is a function of the elastic constants with respect to the material principal axes (x_1, x_2, x_3) and the angle θ; values of elastic constants with respect to coordinates x_1, x_2, x_3 are determined either using a micromechanics theory or test data.

2.4.1.1. Weeks and Sun's approach [26] for finding A_{12} and A_{23}. From Eqs. (2.19) and (2.22) one can find $\bar{\sigma}$ as a function of $\bar{e}^p$, or equivalently plot the curve $\bar{\sigma}$ versus $\bar{e}^p$ for a given angle θ. The value of parameter A_{12} is found by trial and error by ensuring that $\bar{\sigma}$ versus $\bar{e}^p$ curves for various values of θ are close to each other within an acceptable tolerance [26].

We follow a similar procedure to find A_{23}. It is noted that this term was ignored in [26]. For simple shearing deformations in the yz-plane with $\theta = 0$ we have

$$\bar{\sigma} = \sqrt{3A}_{23}\sigma_{yz} \quad de^p_{yz} = d\lambda(A_{23})\sigma_{yz} \tag{2.23}$$

Using Eqs. (2.5) and (2.6) we have

$$d\bar{e}^p = \frac{de^p_{yz}}{2\sqrt{3A_{23}}} \text{ or } \bar{e}^p = \frac{e^p_{yz}}{2\sqrt{3A_{23}}} \tag{2.24}$$

where $e^p_{yz} = e_{yz} - \sigma_{yz}/2G_{yz}$ and recalling that for $\theta = 0$, $G_{yz} = G_{23}$.

2.4.1.2. Alternative approach for finding A_{12} and A_{23}. An alternative approach for finding values of parameters A_{12} and A_{23} as well as the function $\bar{\sigma}(\bar{e}^p)$ is now described. Using the FST method we numerically simulate plane stress deformations of the UFPC under a uniaxial load in the x_2-direction. Thus the only non-zero component of the stress tensor is σ_{22}, and from Eqs. (2.15) and (2.14) we get

$$\bar{\sigma} = \sqrt{\frac{3}{2}}\sigma_{22} \tag{2.25}$$

Theoretically the UFPC will begin to deform plastically as soon as the matrix in one of the three matrix cells of the representative volume element (RVE) starts yielding. This definition gives unrealistically low values of the yield stress of the UFPC and depends on the type of load (e.g., tensile, compressive, simple shearing) applied to the RVE. Here we use computed values of σ_{22} and e_{22} to plot the σ_{22} versus e_{22} curve and take the proof-stress for $e_{22} = 0.0015$ as the value of the yield stress. Recall that the proof stress equals the value of σ_{22} where the straight line parallel to the slope of the σ_{22} versus e_{22} curve at $e_{22} = 0$ (Young's modulus at zero strain) passing through the point ($\sigma_{22} = 0$, $e_{22} = 0.0015$) intersects the σ_{22} versus e_{22} curve. We thus find $\bar{\sigma}_{yield}$ when the UFPC begins to yield as:

$$\bar{\sigma}_{yield} = \sqrt{\frac{3}{2}}\sigma^{PS}_{22} \tag{2.26}$$

where σ^{PS}_{22} equals the proof-stress σ_{22}.

In order to find values of A_{12} and A_{23} we use the FST technique to simulate simple shearing deformations of the UFPC in the x_1x_2- and the x_2x_3-planes. Using the same definition of the yield stress as that adopted in Eq. (2.26) we obtain

$$\bar{\sigma}_{yield} = \sqrt{3A_{12}}\sigma^{PS}_{12} = \sqrt{3A_{23}}\sigma^{PS}_{23} \tag{2.27a, b}$$

We find $\bar{\sigma}_{yield}$ from Eq. (2.26), and then values of parameters A_{12} and A_{23} from Eq. (2.27a,b).

We note that in Weeks and Sun's [26] approach values of parameters A_{12}, A_{23} and $\bar{\sigma}_{yield}$ are determined by considering $\bar{\sigma}$ versus $\bar{e}^p$ curves for the entire range of values of $\bar{e}^p$ considered, and $\bar{\sigma}_{yield} = \bar{\sigma}$ when $\bar{e}^p = 0$. Thus the value of $\bar{\sigma}_{yield}$ is determined after values of A_{12} and A_{23} have been found. The $\bar{\sigma}(\bar{e}^p)$ function is found from the computed $\bar{\sigma}$ versus $\bar{e}^p$ curve by the least squares method. However, in the alternative approach proposed here values of A_{12}, A_{23} and $\bar{\sigma}_{yield}$ are found from those of the proof stresses in uniaxial loading in the transverse direction, and in simple shearing deformations in the x_1x_2- and the x_2x_3-planes. One does not need the $\bar{\sigma}$ versus $\bar{e}^p$ curves for the entire range of values of $\bar{e}^p$.

2.4.2. Pressure-dependent yield surface

We now need to find values of parameters α, A_{12}, A_{23} and $\bar{\sigma}_{yield}$. When using Weeks and Sun's [26] approach we find values of α and A_{12} by ensuring that the $\bar{\sigma}$ versus $\bar{e}^p$ curves for different values of the fiber-orientation angle θ in Fig. 1, and positive and negative values of σ_{xx} are close to each other within the prescribed tolerance. Subsequently, the value of A_{23} is chosen so that the $\bar{\sigma}$ versus $\bar{e}^p$ curve for the simple shearing deformations in the yz-plane is close to the $\bar{\sigma}$ versus $\bar{e}^p$ curve for uniaxial loading.

In the alternative approach proposed here we use the FST technique to compute σ_{22} versus e_{22} curves separately for positive and negative values of σ_{22}, and find $\bar{\sigma}^t_{yield}$ and $\bar{\sigma}^c_{yield}$ from σ^{PS}_{22}. From Eq. (2.17) we get

$$\alpha = \sqrt{\frac{3}{2}}\left\{\frac{\bar{\sigma}^c_{yield} - \bar{\sigma}^t_{yield}}{\bar{\sigma}^c_{yield} + \bar{\sigma}^t_{yield}}\right\}, \quad \bar{\sigma}_{yield} = \sqrt{\frac{3}{2}}\left\{\frac{2\bar{\sigma}^c_{yield}\bar{\sigma}^t_{yield}}{\bar{\sigma}^c_{yield} + \bar{\sigma}^t_{yield}}\right\} \tag{2.28a, b}$$

Values of parameters A_{12} and A_{23} are found by following a procedure similar to that described in Section 2.4.1.2.

3. Numerical results and discussion

3.1. Elastic constants for AS4 fibers

The fiber is modeled as a transversely isotropic material with the fiber axis as the axis of transverse isotropy. With the x_1-axis of a rectangular Cartesian coordinate system taken along the fiber axis, values of five independent elastic moduli of AS4 fibers [21] are listed in Table 1.

3.2. Material parameters for PEEK assuming pressure independent yielding

The PEEK is assumed to be isotropic and its response in the elastic region is taken to be linear. Values of Young's modulus, E^m, and Poisson's ratio, ν^m, obtained from Goldberg and Stouffer [22] for the PEEK tested by Bordonaro [23] equal 4 GPa and 0.35, respectively. The axial stress versus the axial strain curve for PEEK deformed in simple tension at an axial strain rate of 1.0×10^{-6}/s

Table 1
Elastic constants of AS4 carbon fibers.

E_1	$E_2 = E_3$	G_{12}	ν_{12}	ν_{23}
234 GPa	14 GPa	27.6 GPa	0.2	0.25

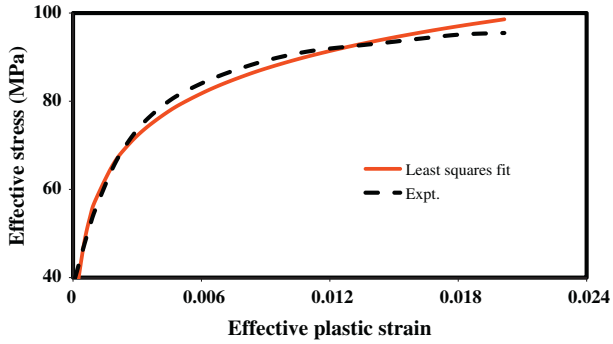

Fig. 2a. Effective stress versus effective plastic strain curve for PEEK obtained from the experimental axial stress versus axial strain curve of [23], and the least squares fit.

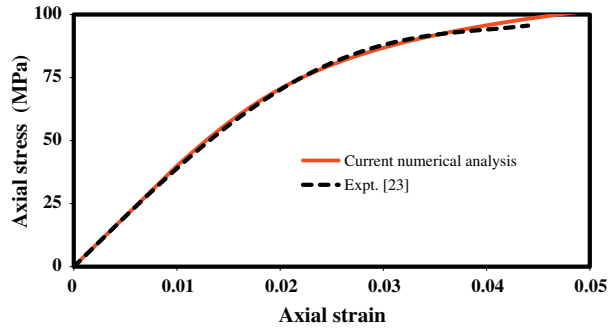

Fig. 2b. Computed and experimental axial stress versus axial strain curves for PEEK polymer.

taken from [22] is exhibited in Fig. 2a. For a uniaxial tension test with the load applied along the x_1-axis, the only non-zero component of the stress tensor is σ_{11}, and from the definition (2.5) of the effective stress, $\sigma_{11} = \bar{\sigma}$. Eq. (2.6) implies that $de^p_{11} = d\bar{e}^p$, and hence $e^p_{11} = \bar{e}^p$. From the axial stress–axial strain curve of Fig. 2a, we find e^p_{11} by using

$$e^p_{11} = e_{11} - \frac{\sigma_{11}}{E} \tag{3.1}$$

and plot the $\bar{\sigma}$ versus $\bar{e}^p$ curve shown in Fig. 2b where it has been tacitly assumed that the yield stress of PEEK in uniaxial tension and compression equals 40 MPa. Assuming that $\bar{\sigma}$ and $\bar{e}^p$ are related by:

$$\bar{e}^p = exp\left(\frac{\bar{\sigma} - A}{N}\right) \tag{3.2}$$

in the range 94 MPa $\geqslant \bar{\sigma} \geqslant$ 40 MPa, values of A and N found by the least squares method and having a regression coefficient of 0.986 are A = 152.7 MPa and N = 13.86 MPa

Eq. (3.2) was verified by numerically analyzing elastoplastic deformations of a bar made of PEEK and pulled in uniaxial tension. The boundary value problem (BVP) was studied using the finite element method (FEM) by implementing the material model for PEEK as a user subroutine in the software ABAQUS. The elastoplastic problem for the matrix is solved iteratively by first assuming that deformations during an incremental load are elastic. The iterative process within a load step at each integration point is stopped when

$$\frac{\|\boldsymbol{e}^{k+1} - \boldsymbol{e}^k\|}{\|\boldsymbol{e}^k\|} \leqslant 1.0E-8, \;\; \|\boldsymbol{e}^k\|^2 = e^k_{ij} e^k_{ij}$$

where k is the iteration number.

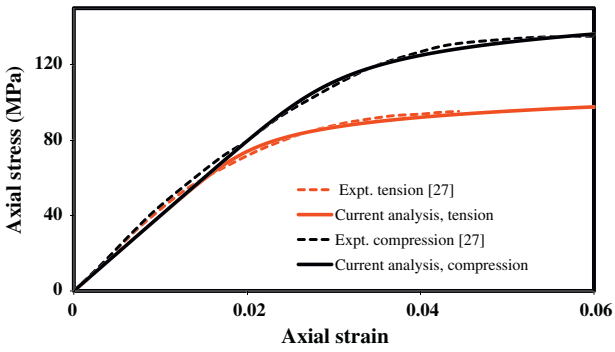

Fig. 3a. Comparison of the computed and the experimental axial stress versus axial strain curves for PEEK polymer deformed in uniaxial tension and compression.

The axial stress versus the axial strain curve so obtained is displayed in Fig. 2b. It is clear that the computed axial stress versus the axial strain curve is very close to the experimental one.

3.3. Material parameters for PEEK assuming pressure dependent yielding

Zheng's [27] experimental uniaxial tension and compression stress–strain curves for PEEK at strain rates of 1.0E−6/s and 1.0E−5/s, respectively, are shown in Fig. 3a. For uniaxial tension test, using Eq. (2.12a), the effective stress $\bar{\sigma}$ and the effective plastic strain $\bar{e}^p$ can be expressed in terms of the axial stress σ_{11} and the axial plastic strain e^p_{11} as:

$$\bar{\sigma} = (1 + \alpha^m)\sigma_{11} \text{ and } \bar{e}^p = \frac{e^p_{11}}{(1+\alpha^m)} = \frac{e_{11} - \frac{\sigma_{11}}{E^m}}{(1+\alpha^m)} \tag{3.3}$$

Similarly, for uniaxial compressive deformations, we have

$$\bar{\sigma} = (1 - \alpha^m)|\sigma_{11}| \text{ and } \bar{e}^p = \frac{|e_{11}| - \frac{|\sigma_{11}|}{E^m}}{(1-\alpha^m)} \tag{3.4}$$

From the experimental uniaxial stress strain curves for tension and compression tests, the effective stress and the effective plastic strain are evaluated using Eqs. (3.3) and (3.4). In Weeks and Sun's approach, the value of α^m is found by adopting an iterative approach so that the effective stress versus the effective plastic strain curves for tension and compression tests overlap each other within an acceptable tolerance. In order to find the difference (distance) between the two curves, fourth-order polynomials are fitted by the least squares method to the effective stress versus the effective plastic strain curves for tension and compression data. The percentage difference between the two curves was found by using,

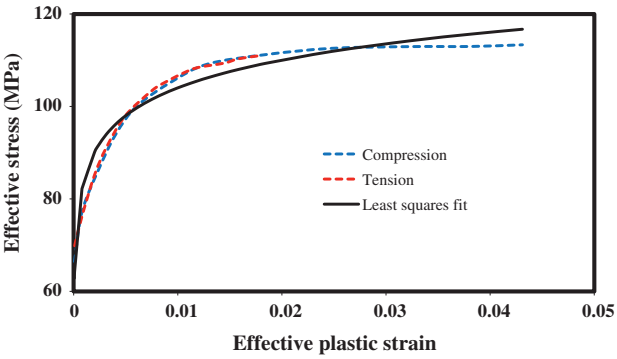

Fig. 3b. Effective stress versus effective plastic strain curve for PEEK obtained from the experimental axial stress versus axial strain curve of [27], and the least squares fit.

$$\% \text{ Difference} = \sqrt{\frac{\sum_i \left(\bar{\sigma}_i^t - \bar{\sigma}_i^c\right)^2}{\sum_i \left(\bar{\sigma}_i^t\right)^2}} 100 \tag{3.5}$$

where $\bar{\sigma}_i^t$ and $\bar{\sigma}_i^c$ are the effective stress values from tension and compression tests, respectively, corresponding to the effective plastic strain $\bar{e}_i^p$. The entire range (0–3%) of $\bar{e}^p$ was divided into 30 equal segments and values at the mid-point of a segment were used in Eq. (3.5). For an error of 1.7%, the iterative procedure gave $\alpha^m = 0.1645$. Fig. 3b shows the effective stress versus the effective plastic strain curve derived from the uniaxial compression and tension test data of Zheng [27], and that obtained from the numerical experiments using $\alpha^m = 0.1645$ and the simulation of uniaxial tensile and compressive deformations with the software ABAQUS.

We also employed the alternative approach to find the value of α^m by using values of the proof stress as the yield stress in uniaxial compression and tension tests. The expression for α^m in terms of the proof stress in tension, σ_t^{PS}, and the proof stress in compression, σ_c^{PS}, obtained from Eqs. (3.3) and (3.4) is:

$$\alpha^m = \left\{\frac{\sigma_c^{PS} - \sigma_t^{PS}}{\sigma_c^{PS} + \sigma_t^{PS}}\right\} \tag{3.6}$$

From the experimental curves depicted in Fig. 3a, we found that $\sigma_t^{PS} = 57$ MPa and $\sigma_c^{PS} = 73$ MPa. Substituting these values for σ_t^{PS} and σ_c^{PS} in the expression (3.6) for α^m, we get $\alpha^m = 0.123$. For $\alpha^m = 0.123$ the difference between the effective stress versus the effective plastic strain curves derived from simulations of the uniaxial tensile and compressive deformations and using definition (3.5) was found to be 16.6% for effective plastic strain in the range 0–3.0%. As mentioned earlier Weeks and Sun's [26] approach uses the entire set of data for $0 \leqslant \bar{e}^p \leqslant 0.03$ whereas the present approach uses values of proof stresses which vary with the definition of the proof stress. For example, one could define the proof stress as the stress corresponding to the strain of 0.13% rather than 0.15%.

Using the relation (3.2) values of A and N were found by fitting a curve by the least squares method to the effective stress versus the effective plastic strain curves derived from the test data of Zheng [27]. With a regression coefficient of 0.954 and $\alpha^m = 0.1645$, we obtained $A = 144.0$ MPa and $N = 8.69$ MPa. In Fig. 3a we have compared the experimental uniaxial stress strain curves with those obtained by implementing the material model for PEEK as a user subroutine in ABAQUS and employing $\alpha^m = 0.1645$, $A = 144.0$ MPa and $N = 8.69$ MPa. It is evident that the computed axial stress versus the axial strain curves for uniaxial compressive and tensile deformations are close to the corresponding experimental ones.

3.4. Elasto-plastic properties of the composite

3.4.1. Validity of the FST approach for elasto-plastic deformations

Given values of elastic moduli of the fiber and the matrix, and the effective stress, $\bar{\sigma}$, of the matrix as a function of the effective plastic strain, $\bar{e}^{pm}$, for the matrix, we find values of A_{12}, A_{23} and $\bar{\sigma}(\bar{e}^p)$ for the UFPC. A user defined subroutine based on the FST method described in Appendix has been implemented in the FE software, ABAQUS. The three matrix cells deform elasto-plastically and the fiber cell elastically.

In order to determine the elastoplastic material response of the AS4/PEEK composite two material models for the polymer are considered; one assumes that the von Mises yield surface in which plastic deformations are independent of the hydrostatic pressure [24] (discussed in Section 2.2.1) and the other assumes that the hydrostatic pressure contributes to plastic deformations [27] (discussed in Section 2.2.2). The elastic–plastic properties for pressure insensitive and pressure sensitive polymer are given in Sections 3.2 and 3.3, respectively. Using material properties of the constituents and the volume fraction of fibers we simulated uniaxial deformations of the composite. Since the composite specimen is expected to deform homogeneously only one FE is used to simulate these tests.

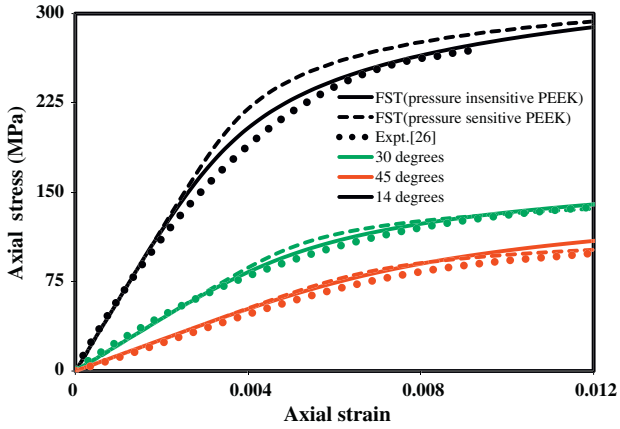

Fig. 4. For $v^f = 0.6$, comparison of the computed axial stress–axial strain curves for off-axis loading using the FST approach with the experimental curves of Weeks and Sun [26].

For $v^f = 0.6$, Fig. 4 compares the computed axial stress versus the axial strain curves for off-axis loading (e.g., see Fig. 1) with experimental results reported by Weeks and Sun [26]. It is clear that for $\theta = 14°$ the axial stress versus the axial strain response obtained using the pressure independent von Mises yield surface for the polymer is in better agreement with the experimental data than that when the polymer is modeled with the pressure dependent Drucker–Prager yield surface. However, for $\theta = 30°$ and 45° the pressure sensitive and pressure insensitive yield surfaces give stresses very close to the experimental values. For $\theta = 14°$, σ_{11} is much greater than σ_{22} and matrix's deformations are negligible. For $\theta = 30°$ and 45°, because of the large volume fraction of fibers, the matrix's deformations play a less noticeable role and the differences in the compressive and tensile deformations of the polymer is less noticeable in the axial stress–axial strain curves. Experimental results for simple shearing loading of this composite would have provided a better check on the two yield criteria but we have not found them.

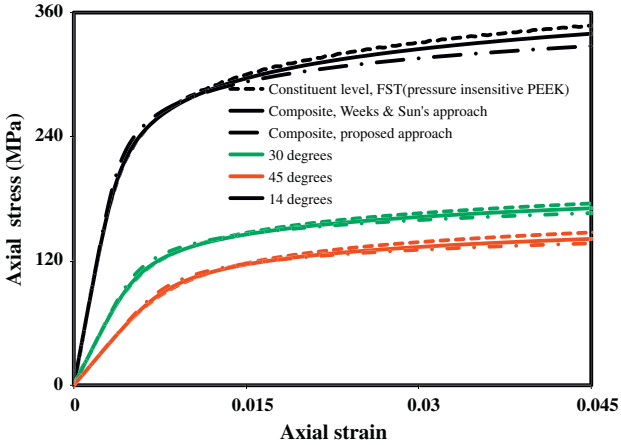

Fig. 5. For $v^f = 0.6$, comparison of axial stress–axial strain response for off-axis loading obtained from the FST method with the response of pressure insensitive yielding of composites using values of parameters determined from the two approaches.

3.4.2. Values of material parameters for the homogenized composite

Values of material parameters appearing in the yield surfaces of the UFPC are determined with the FST method. For $v^f = 0.6$, and using the techniques discussed in Section 3.4, we get the following results:

(a) **Pressure independent yield surface**
(i) Weeks and Sun's approach
$A_{12} = 7.5$ $A_{23} = 8.5$ $A = 496.6$ MPa $N = 35.2$ MPa
(ii) Present approach
$A_{12} = 5.45$ $A_{23} = 6.47$ $A = 388.5$ MPa $N = 24.4$ MPa
(b) **Pressure dependent yield surface**
(i) Weeks and Sun's approach
$A_{12} = 2.1$ $A_{23} = 2.2$ $A = 250.0$ MPa $N = 15.4$ MPa
(ii) Present approach
$A_{12} = 3.22$ $A_{23} = 3.47$ $A = 303.7$ MPa $N = 16.7$ MPa

Here $\alpha = 0.544$ found by the present approach is used in weeks and Sun's method to find A_{12} and A_{23}.

3.4.3. Comparison of results from the FST method with those from the homogenized composite

In Fig. 5 we compare the axial stress versus the axial strain curves for off-axis loading obtained from the FST method with the axial stress versus the axial strain response for the pressure insensitive yielding of composites using above-listed values of material parameters. It is clear that the three sets of curves are close to each other.

For the pressure sensitive yield surface, Fig. 6 compares the axial stress versus the axial strain curves for off-axis loading of a lamina obtained using the FST method with those computed by using the above-listed values of material parameters. Again, the three sets of curves are close to each other.

3.4.4. Dependence of the yield surface upon the fiber volume fraction

We only use the von Mises yield criterion for the matrix and the composite with the composite modeled as a transversely isotropic material and the fiber axis as the axis of transverse isotropy; results for the pressure dependent yield surface can be similarly obtained. Furthermore, we seek an expression for the effective stress of the composite with variables A and N depending upon the volume fraction of the fibers. We have exhibited in Fig. 7a and b the dependence of parameters A, N, A_{12} and A_{23} upon the volume fraction of fibers ranging from 0.3 to 0.75. The least squares cubic polynomial fits to the computed values of these variables are listed as insets in the figures. It is clear that values of all four parameters rapidly increase with an increase in the value of the volume fraction of fibers.

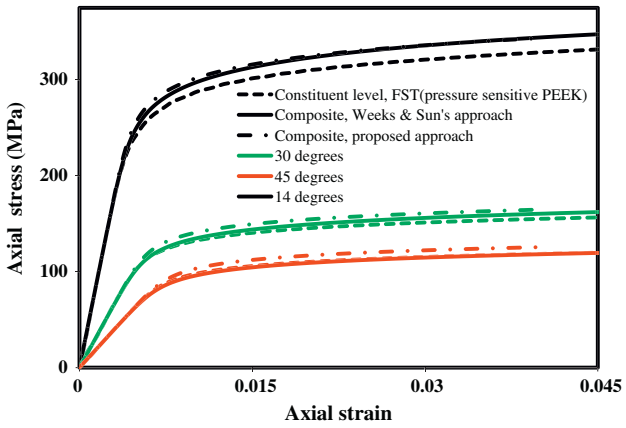

Fig. 6. For $v^f = 0.6$, comparison of axial stress–axial strain response for off-axis loading obtained from the FST method with the response of pressure insensitive yielding of composites using values of parameters determined from the two methods.

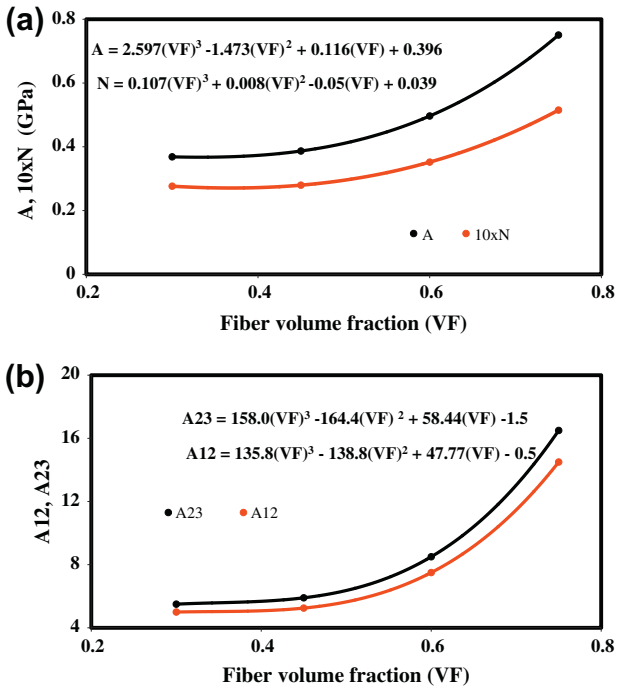

Fig. 7. Variation with the fiber volume fraction of the parameters (a) A and N, and (b) A_{12} and A_{23} appearing in the yield surface.

4. Conclusions

We have used a micromechanics approach (i.e., the free shear traction method proposed by Robertson and Mall that is a modification of Aboudi's method of cells) to find values of material parameters for elasto-plastic deformations of AS4/PEEK composite modeled by two yield criteria – the von Mises that stipulates that plastic deformations are independent of the hydrostatic pressure and the Drucker–Prager that includes dependence of the yield surface upon the hydrostatic pressure. Whereas the von Mises yield surface is quadratic in deviatoric stresses the other one has a term linear in the pressure.

For uniaxial elasto-plastic deformations of the composite lamina and fibers making an angle θ with the axis of loading, the axial stress versus the axial strain curves computed with the von Mises yield criterion for the PEEK agree better with the experimental results of Weeks and Sun than those derived by assuming that the yield criterion is pressure dependent. Assuming that the plastic deformations of the composite are also independent of the hydrostatic pressure, we have found values as a function of the volume fraction of fibers of the two material parameters in the yield surface and the two material parameters that characterize strain hardening of the composite.

The pressure independent yield surface for the AS4/PEEK composite studied herein is given by:

$$\bar{\sigma} = \sqrt{3F(\sigma_{ij})} = A + N\ln(\bar{e}^p)$$

where

$$F(\sigma_{ij}) = \frac{1}{2}\left[(\sigma_{22}-\sigma_{33})^2 + 2A_{23}\sigma_{23}^2 + 2A_{12}(\sigma_{13}^2+\sigma_{12}^2)\right]$$

$$A = 2.597(\mathrm{VF})^3 - 1.473(\mathrm{VF})^2 + 0.116(\mathrm{VF}) + 0.396$$

$$N = 0.107(\mathrm{VF})^3 + 0.008(\mathrm{VF})^2 - 0.050(\mathrm{VF}) + 0.039$$

$$A_{23} = 158.0(\mathrm{VF})^3 - 164.4(\mathrm{VF})^2 + 58.44(\mathrm{VF}) - 1.5$$

$$A_{12} = 135.8(\mathrm{VF})^3 - 138.8(\mathrm{VF})^2 + 47.77(\mathrm{VF}) - 0.5$$

and VF equals the volume fraction of the fibers with VF between 0.3 and 0.75. By following a procedure similar to that used here and simulating homogeneous deformations of the UFPC at different strain rates one can quantify the dependence of the yield stress of the UFPC upon the strain rate characteristics of the fiber and the matrix.

Acknowledgements

This research was sponsored by the Army Research Laboratory and was accomplished under Cooperative Agreement Number W911NF-06-2-0014. The views and conclusions contained in this document are those of the authors and should not be interpreted as representing official policies, either expressed or implied, of the Army Research Laboratory or the US Government. The US Government is authorized to reproduce and distribute reprints for Government purposes notwithstanding any copyright notation hereon. The work was also partially supported by the Office of Naval Research Grant N00014-1-06-0567 to Virginia Polytechnic Institute and State University with Dr. Y.D.S. Rajapakse as the program manager.

Appendix A

A.1. Comparison of results between Mori–Tanaka and the FST techniques

The FST approach used to establish values of material parameters is briefly reviewed. The FST approach is a modification of the method of cells (MoC) and assumes that at the interfaces between the four cells in the RVE a normal stress does not induce shear stresses thereby simplifying the homogenization scheme. Robertson and Mall [15] have shown that values of material parameters derived by using the FST method are close to those obtained by using the MoC and that the FST approach requires less computational effort than the MoC. The maximum difference of 10% was found in the values of the in-plane shear modulus derived from the two approaches over a range of fiber volume fractions of practical interest. Robertson and Mall [16] have also used the FST approach to homogenize material properties of a composite with visco-plastic constituents. Gardner [28] has generalized the MoC to include fiber/matrix debonding.

In the FST approach a cylindrical RVE of square cross-section is considered with the cross-section divided into two square and two rectangular cells; e.g., see Fig. 8. Each cell is made of a homogeneous material and is assumed to deform uniformly. The material of one rectangular cell is fiber and that of the remaining three cells the matrix.

The displacement continuity conditions at the interfaces between cells, expressed in terms of strain components, are listed below [15,16].

$$\begin{aligned}
&\varepsilon_{11}^{F} = \bar{\varepsilon}_{11} \quad \varepsilon_{11}^{M1} = \bar{\varepsilon}_{11} \quad \varepsilon_{11}^{M2} = \bar{\varepsilon}_{11} \quad \varepsilon_{11}^{M3} = \bar{\varepsilon}_{11}\\
&a\varepsilon_{22}^{F} + b\varepsilon_{22}^{M1} = a\varepsilon_{22}^{M3} + b\varepsilon_{22}^{M2} = (a+b)\bar{\varepsilon}_{22}\\
&a\varepsilon_{33}^{F} + c\varepsilon_{33}^{M3} = a\varepsilon_{33}^{M1} + c\varepsilon_{33}^{M2} = (a+c)\bar{\varepsilon}_{33}\\
&\gamma_{12}^{F} = \gamma_{12}^{M3} \quad \gamma_{12}^{M1} = \gamma_{12}^{M2}\\
&a\gamma_{12}^{F} + b\gamma_{12}^{M1} = (a+b)\bar{\gamma}_{12}\\
&\gamma_{13}^{F} = \gamma_{13}^{M1} \quad \gamma_{13}^{M2} = \gamma_{13}^{M3}\\
&a\gamma_{13}^{F} + c\gamma_{13}^{M3} = (a+b)\bar{\gamma}_{13}\\
&a^2\gamma_{23}^{F} + ab\gamma_{23}^{M1} + bc\gamma_{23}^{M2} + ac\gamma_{23}^{M3} = (a+b)(a+b)\bar{\gamma}_{23}
\end{aligned} \tag{A.1}$$

In Eq. (A.1) strain components with an over bar represent the average strains in the RVE.

The continuity of resultant forces at the interfaces between the regions gives the following equations wherein superscripts F and M stand for the fiber and the matrix, respectively, and the additional superscripts 1, 2 and 3 correspond to the cell number.

$$\begin{aligned}
&\sigma_{22}^{F} = \sigma_{22}^{M1} \quad \sigma_{22}^{M2} = \sigma_{22}^{M3} \quad \sigma_{33}^{F} = \sigma_{33}^{M3} \quad \sigma_{33}^{M1} = \sigma_{33}^{M2}\\
&a\tau_{12}^{F} + c\tau_{12}^{M3} = a\tau_{12}^{M1} + c\tau_{12}^{M2}\\
&a\tau_{13}^{F} + b\tau_{13}^{M1} = a\tau_{13}^{M3} + b\tau_{13}^{M2}\\
&\tau_{23}^{F} = \tau_{23}^{M3} = \tau_{23}^{M2} = \tau_{23}^{M1}
\end{aligned} \tag{A.2}$$

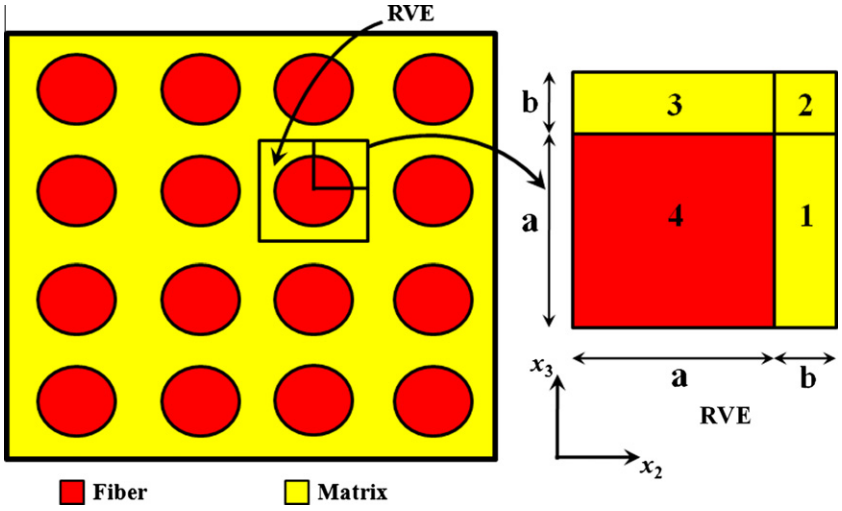

Fig. 8. Left: cross-section of a UFPC with uniform arrangement of fibers; right: representation of the cross-section by four cells, three of which are made of the matrix and the fourth one of the fiber; $a = \sqrt{v^f}$, $b = 1 - a$

Using constitutive equations for the fiber and the matrix Eqs. (A.1) and (A.2) can be re-written as:

$$\left\{\begin{Bmatrix}\varepsilon_{22}^{F}\\ \varepsilon_{33}^{F}\end{Bmatrix}\begin{Bmatrix}\varepsilon_{22}^{M1}\\ \varepsilon_{33}^{M1}\end{Bmatrix}\begin{Bmatrix}\varepsilon_{22}^{M2}\\ \varepsilon_{33}^{M2}\end{Bmatrix}\begin{Bmatrix}\varepsilon_{22}^{M3}\\ \varepsilon_{33}^{M3}\end{Bmatrix}\right\} = [\mathrm{NORMAL}]\left\{\begin{matrix}(a+b)\bar{\varepsilon}_{22}\\ (a+b)\bar{\varepsilon}_{22}\\ (a+b)\bar{\varepsilon}_{33}\\ (a+b)\bar{\varepsilon}_{33}\\ \left(C_{21}^{M}-C_{21}^{F}\right)\bar{\varepsilon}_{11}\\ 0\\ \left(C_{31}^{M}-C_{31}^{F}\right)\bar{\varepsilon}_{11}\\ 0\end{matrix}\right\} \tag{A.3}$$

where

$$[\mathrm{NORMAL}] = \begin{bmatrix} a & 0 & b & 0 & 0 & 0 & 0 & 0\\ 0 & 0 & 0 & 0 & b & 0 & a & 0\\ 0 & a & 0 & 0 & 0 & 0 & 0 & b\\ 0 & 0 & 0 & a & 0 & b & 0 & 0\\ C_{22}^{F} & C_{23}^{F} & -C_{22}^{M} & -C_{23}^{M} & 0 & 0 & 0 & 0\\ 0 & 0 & 0 & 0 & C_{22}^{M} & C_{23}^{M} & -C_{22}^{M} & -C_{23}^{M}\\ C_{32}^{F} & C_{33}^{F} & 0 & 0 & 0 & 0 & -C_{32}^{M} & -C_{33}^{M}\\ 0 & 0 & C_{32}^{M} & C_{33}^{M} & -C_{32}^{M} & -C_{33}^{M} & 0 & 0 \end{bmatrix}^{-1}$$

Furthermore,

$$\left\{\begin{Bmatrix}\gamma_{23}^{F}\\ \gamma_{13}^{F}\\ \gamma_{12}^{F}\end{Bmatrix}\begin{Bmatrix}\gamma_{23}^{M1}\\ \gamma_{13}^{M1}\\ \gamma_{12}^{M1}\end{Bmatrix}\begin{Bmatrix}\gamma_{23}^{M2}\\ \gamma_{13}^{M2}\\ \gamma_{12}^{M2}\end{Bmatrix}\begin{Bmatrix}\gamma_{23}^{M3}\\ \gamma_{13}^{M3}\\ \gamma_{12}^{M3}\end{Bmatrix}\right\} = [\mathrm{SHEAR}]\left\{\begin{matrix}0\\ 0\\ (a+b)\bar{\gamma}_{12}\\ 0\\ 0\\ (a+b)\bar{\gamma}_{13}\\ (a+b)(a+b)\bar{\gamma}_{23}\\ 0\\ 0\\ 0\\ 0\\ 0\end{matrix}\right\} \tag{A.4}$$

where

As indicated below, inelastic deformations of the matrix are accommodated by incorporating plastic strains in Eqs. (A.3) and (A.4).

$$\left\{\begin{Bmatrix}\varepsilon_{22}^{F}\\ \varepsilon_{33}^{F}\end{Bmatrix}\begin{Bmatrix}\varepsilon_{22}^{M1}\\ \varepsilon_{33}^{M1}\end{Bmatrix}\begin{Bmatrix}\varepsilon_{22}^{M2}\\ \varepsilon_{33}^{M2}\end{Bmatrix}\begin{Bmatrix}\varepsilon_{22}^{M3}\\ \varepsilon_{33}^{M3}\end{Bmatrix}\right\} = [\mathrm{NORMAL}]\left\{\begin{matrix}(a+b)\bar{\varepsilon}_{22}\\ (a+b)\bar{\varepsilon}_{22}\\ (a+b)\bar{\varepsilon}_{33}\\ (a+b)\bar{\varepsilon}_{33}\\ \left(C_{21}^{M}-C_{21}^{F}\right)\bar{\varepsilon}_{11}-\left[C_{2i}^{M}\right]\{\varepsilon^{MP1}\}\\ \left[C_{2i}^{M}\right]\{\varepsilon^{MP2}-\varepsilon^{MP3}\}\\ \left(C_{31}^{M}-C_{31}^{F}\right)\bar{\varepsilon}_{11}-\left[C_{3i}^{M}\right]\{\varepsilon^{MP3}\}\\ \left[C_{3i}^{M}\right]\{\varepsilon^{MP1}-\varepsilon^{MP2}\}\end{matrix}\right\} \tag{A.5}$$

and

$$\left\{\begin{Bmatrix}\gamma_{23}^{F}\\ \gamma_{13}^{F}\\ \gamma_{12}^{F}\end{Bmatrix}\begin{Bmatrix}\gamma_{23}^{M1}\\ \gamma_{13}^{M1}\\ \gamma_{12}^{M1}\end{Bmatrix}\begin{Bmatrix}\gamma_{23}^{M2}\\ \gamma_{13}^{M2}\\ \gamma_{12}^{M2}\end{Bmatrix}\begin{Bmatrix}\gamma_{23}^{M3}\\ \gamma_{13}^{M3}\\ \gamma_{12}^{M3}\end{Bmatrix}\right\} = [\mathrm{SHEAR}]\left\{\begin{matrix}0\\ 0\\ (a+b)\bar{\gamma}_{12}\\ 0\\ 0\\ (a+b)\bar{\gamma}_{13}\\ (a+b)(a+b)\bar{\gamma}_{23}\\ C_{66}^{M}\left[c\gamma_{12}^{MP3}-a\gamma_{12}^{MP1}-c\gamma_{12}^{MP2}\right]\\ C_{55}^{M}\left[b\gamma_{13}^{MP1}-a\gamma_{13}^{MP3}-b\gamma_{13}^{MP2}\right]\\ -C_{44}^{M}\gamma_{23}^{MP3}\\ -C_{44}^{M}\gamma_{23}^{MP1}\\ -C_{44}^{M}\gamma_{23}^{MP2}\end{matrix}\right\} \tag{A.6}$$

where [NORMAL] and [SHEAR] are as defined in Eqs. (A.4) and (A.5) and

$$\{\varepsilon^{MPi}\} = \begin{Bmatrix}\varepsilon_{1}^{MPi}\\ \varepsilon_{2}^{MPi}\\ \varepsilon_{3}^{MPi}\end{Bmatrix}$$

$$[\mathrm{SHEAR}] = \begin{bmatrix} 0 & 0 & 1 & 0 & 0 & 0 & 0 & 0 & 0 & 0 & 0 & -1\\ 0 & 0 & 0 & 0 & 0 & 1 & 0 & 0 & -1 & 0 & 0 & 0\\ 0 & 0 & a & 0 & 0 & b & 0 & 0 & 0 & 0 & 0 & 0\\ 0 & 1 & 0 & 0 & -1 & 0 & 0 & 0 & 0 & 0 & 0 & 0\\ 0 & 0 & 0 & 0 & 0 & 0 & 0 & 1 & 0 & 0 & -1 & 0\\ 0 & a & 0 & 0 & 0 & 0 & 0 & 0 & 0 & 0 & b & 0\\ a^{2} & 0 & 0 & ab & 0 & 0 & b_{2} & 0 & 0 & ab & 0 & 0\\ 0 & 0 & aC_{66}^{F} & 0 & 0 & -aC_{66}^{M} & 0 & 0 & -bC_{66}^{M} & 0 & 0 & bC_{66}^{M}\\ 0 & aC_{55}^{F} & 0 & 0 & bC_{55}^{M} & 0 & 0 & -bC_{55}^{M} & 0 & 0 & -aC_{55}^{M} & 0\\ C_{44}^{F} & 0 & 0 & 0 & 0 & 0 & 0 & 0 & 0 & -C_{44}^{M} & 0 & 0\\ C_{44}^{F} & 0 & 0 & -C_{44}^{M} & 0 & 0 & 0 & 0 & 0 & 0 & 0 & 0\\ C_{44}^{F} & 0 & 0 & 0 & 0 & -C_{44}^{M} & 0 & 0 & 0 & 0 & 0 & 0 \end{bmatrix}^{-1}$$

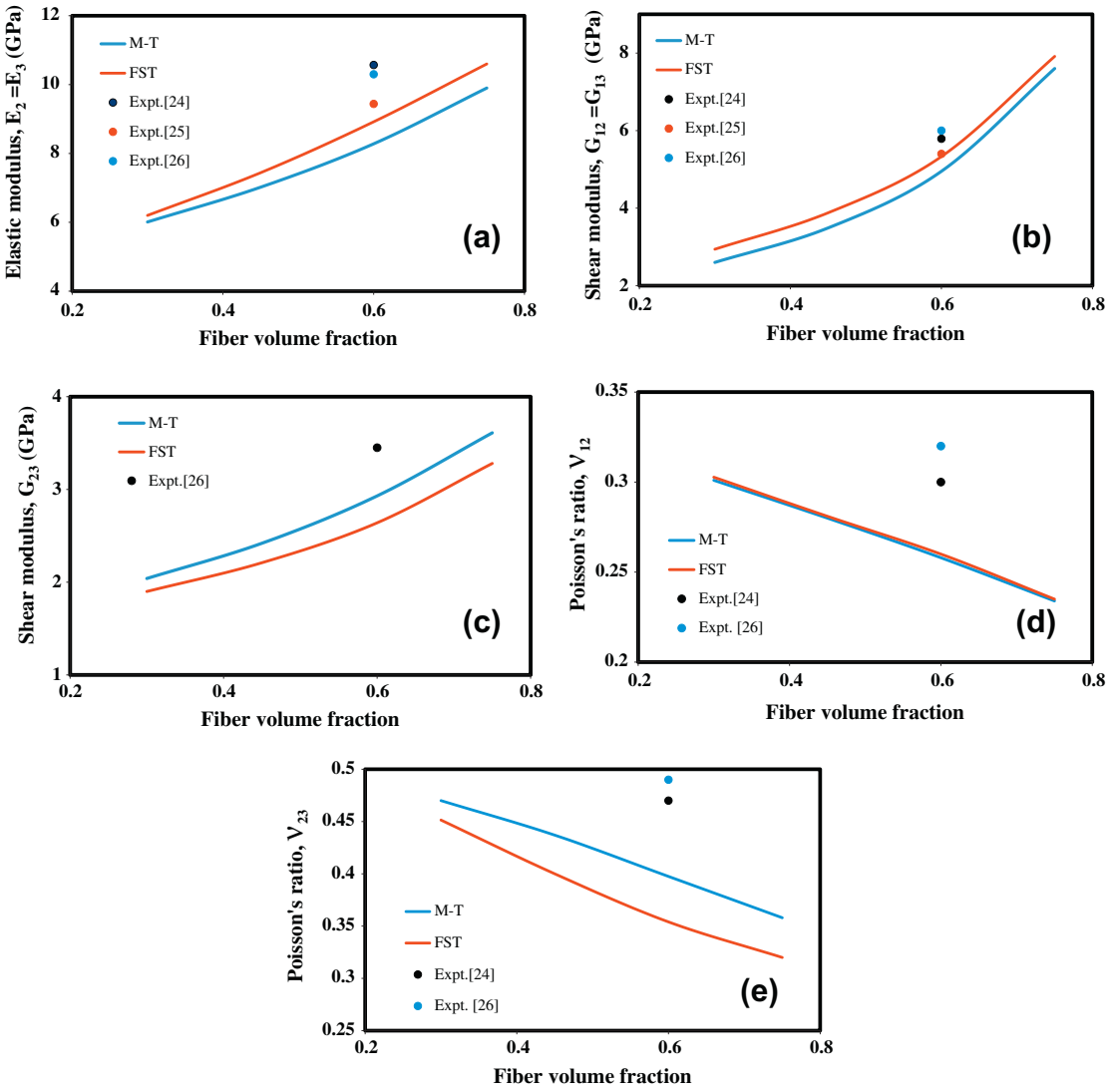

Fig. 9. Using different micromechanics approaches, computed variation with v^f of (a) the elastic modulus $E_2 = E_3$, (b) $G_{12} = G_{13}$, (c) G_{23}, (d) Poisson's ratio v_{12}, and (e) Poisson's ratio v_{23} obtained using M–T = Mori–Tanaka, FST = free shear traction. Test data from Refs. [24–26] are shown in the figure.

Table 2
Values of material parameters for the matrix.

Elastic modulus	Poisson's ratio	Yield stress	Hardening modulus
45 GPa	0.35	0.15 GPa	1.28 GPa

Table 3
Elastic constants of carbon fibers.

E_1	$E_2 = E_3$	$G_{12} = G_{13}$	$v_{12} = v_{13}$	v_{23}
224 GPa	14 GPa	14 GPa	0.2	0.25

$$\left[C_{Ji}^{M}\right] = \left[C_{J1}^{M} \quad C_{J2}^{M} \quad C_{J3}^{M}\right]$$

C_{ij}^{M} and C_{ij}^{F} stand for elastic constants of the matrix and the fiber, respectively.

Fig. 9a–e compares values of the elastic constants predicted by the FST method with those found by using the M–T scheme, and available experimental values [24–26]. Results from the two approaches agree qualitatively and are, in general, close to each other for the fiber volume fraction ranging between 0.3 and 0.75.

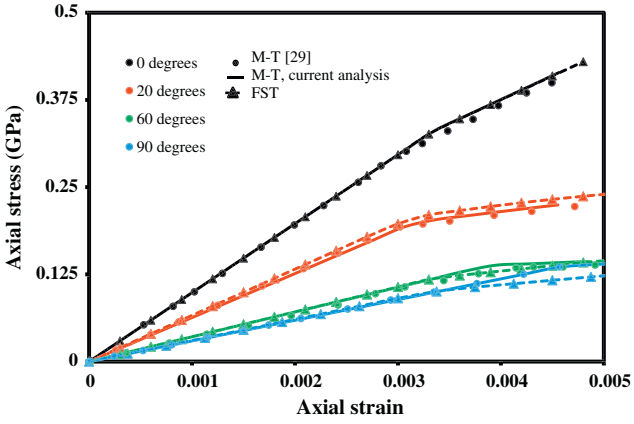

Fig. 10. For $v^f = 0.3$, comparison of the axial stress versus the axial strain curves for off-axis loading computed using the incremental M–T and the FST methods.

Next we compare results of elasto-plastic deformations obtained using the incremental Mori–Tanaka (M–T) and the FST methods. The algorithm for the M–T method has been given by

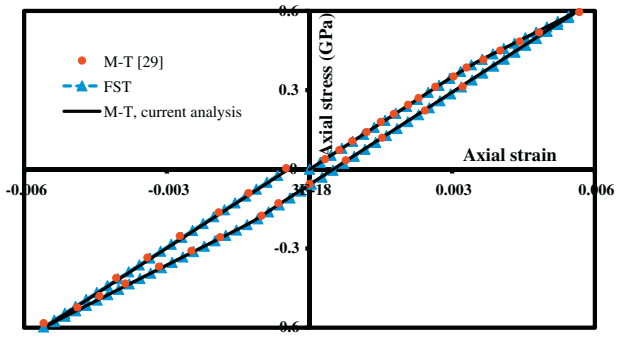

Fig. 11. For $v^f = 0.4$, comparison of the axial stress versus the axial strain curves for cyclic loading from the incremental M–T and the FST methods.

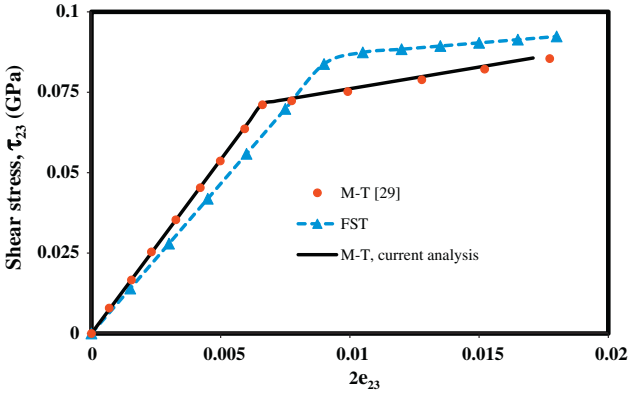

Fig. 12. For $v^f = 0.4$, comparison of the shear stress versus the shear strain curves computed using the incremental M–T and the FST approaches.

Pettermann et al. [29], and we study the same composite (carbon fiber reinforced metal matrix) as that analyzed in [29]. It is assumed that only the matrix deforms plastically, and it can be modeled as an elasto-plastic material obeying the von-Mises yield criterion with the effective stress an affine function of the effective plastic strain (i.e., affine strain hardening). Values of material parameters for the matrix taken from [29] are listed in Table 2, and those for the carbon fiber given in Table 3 are slightly different from those listed in Table 1. Here we have used values of parameters from Ref. [29] so that we can compare our computed results with those of Pettermann et al. [29].

In Fig. 10 we have plotted the axial stress versus the axial strain curves for off-axis loading of a lamina obtained by using the two approaches. In general, the results from the two methods agree well with each other. However, when fibers are inclined at either 60° or 90° with the loading axis, yielding occurs at a lower value of the strain for the FST method than that with the incremental M–T approach. In Figs. 11 and 12, we have compared results for the cyclic loading along the fiber direction and for the in-plane shear loading. The initial slope, G_{23} of the shear stress versus the shear strain curve from the incremental M–T method is higher than that of the curve computed with the FST approach. The yield stress obtained from results using the FST method is higher than that deduced from results of the M–T approach, and the FST method predicts a lower value of the strain hardening modulus than the input value. Thus the two micromechanics theories that give very close results for axial deformations of a composite lamina do not provide close values of the yield stress and the hardening modulus for in-plane shear deformations.

We note that Jiang and Batra [33–35] used the energy equivalence principle and the Mori–Tanaka method to homogenize particulate composites containing elastic–plastic inclusions and a viscoleastic matrix.

References

[1] Torquato S. Random heterogeneous media. New York: Springer-Verlag; 2002.
[2] Suquet PM. Continuum micro-mechanics. New York: Springer-Verlag; 1997.
[3] Bensoussan A, Lions JL, Papanicolaou G. Asymptotic analysis for periodic structures. New York: North-Holland Publishing Company; 1978.
[4] Nemat-Nasser S, Hori M. Micromechanics: overall properties of heterogeneous materials. 2nd ed. Amsterdam: North Holland; 1999.
[5] Mura T. Micromechanics of defects in solids. New York: Kluwer Academic Press; 1987.
[6] Aboudi J. Mechanics of composite materials. Amsterdam: Elsevier Science Publication; 1991.
[7] Tsai SW, Hahn HT. Introduction to composite materials. Lancaster PA: Technomic Publication; 1980.
[8] Hyer MW. Stress analysis of fiber-reinforced composite materials. Lancaster PA: Destech Pubs Inc.; 2008.
[9] Reifsnider KK, Case SW. Damage tolerance and durability in material systems. New York: Wiley-Interscience; 2002.
[10] Charalambakis N. Homogenization techniques and micromechanics. A survey and perspectives. Trans ASME Appl Mech Rev 2010;63:030803–10.
[11] Love BM, Batra RC. Determination of effective thermomechanical parameters of a mixture of two thermoviscoplastic constituents. Int J Plast 2006;22:1026–61.
[12] Bridgman PW. Studies in large plastic flow and fracture with special emphasis on the effects of hydrostatic pressure. New York: McGraw-Hill; 1952.
[13] Caddell RM, Raghava RS, Atkins AG. Pressure dependent yield criteria for polymers. Mater Sci Eng 1974;13:113–20.
[14] Hu LW, Pae KD. Inclusion of the hydrostatic stress component in formulation of the yield condition. J Frank Inst 1963;6:491–502.
[15] Robertson DD, Mall S. Micromechanical relations for fiber-reinforced composites. J Compos Technol Res 1993;15:181–91.
[16] Robertson DD, Mall S. Micromechanical analysis for thermo-viscoplastic behavior of unidirectional fibrous composites. Compos Sci Technol 1994;50:483–96.
[17] Gavazzi AC, Lagoudas DC. On the numerical evaluation of Eshelby's tensor and its application to elastoplastic fibrous composites. Comput Mech 1991;7:13–9.
[18] Aboudi J. Micromechanical analysis of composites by the method of cells. Trans ASME Appl Mech Rev 1989;42:193–221.
[19] Hill R. The mathematical theory of plasticity. New York: Oxford University Press; 1998.
[20] Spencer AJM. Plasticity theory for fiber-reinforced composites. J Eng Math 1992;26:107–18.
[21] Chen JK, Allahdadi FA, Sun CT. A quadratic yield function for fiber-reinforced composites. J Compos Mater 1997;31:788–811.
[22] Goldberg RK, Stouffer DC. Strain rate dependent analysis of a polymer matrix composite utilizing a micromechanics approach. J Compos Mater 2002;36:773–93.
[23] Bordonaro CM. Rate dependent mechanical behavior of high strength plastics: experiment and modeling. PhD Dissertation. Troy, New York: Rensselaer Polytechnic Institute; 1995.
[24] Kyriakides S, Arseculeratne R, Perry E, Liechti K. On the compressive failure of fiber reinforced composites. Int J Solids Struct 1995;32:689–738.
[25] Jen MHR, Lee CH. Strength and life in thermoplastic composite laminates under static and fatigue loads. Part I: experimental. Int J Fatig 1998;20:605–15.
[26] Weeks CA, Sun CT. Modeling non-linear rate-dependent behavior in fiber-reinforced composites. Compos Sci Technol 1998;58:603–11.
[27] Zheng X. Nonlinear strain rate dependent composite model for explicit finite element analysis. PhD Dissertation. Akron, Ohio: University of Akron; 2006.
[28] Gardner, J.P. 1994, Micromechanical modeling of composite materials in finite element analysis using an embedded cell approach. M.Sc. thesis. Cambridge, Massachusetts: MIT.
[29] Pettermann HE, Plankensteiner AF, Boehm HJ, Rammerstorfer FG. A thermo–elasto-plastic constitutive law for inhomogeneous materials based on an incremental Mori–Tanaka approach. Comput Struct 1999;71:197–214.
[30] Hinton MJ, Kaddour AS, Soden PD. Evaluation of failure prediction in composite laminates: background to 'part C' of the exercise. Compos Sci Technol 2004;64:321–7.
[31] Chen JK, Sun CT. A plastic potential suitable for anisotropic fiber composites. J Compos Mater 1993;27:1379–90.
[32] Cho J, Fenner J, Werner B, Daniel IM. A constitutive model for fiber-reinforced polymer composites. J Compos Mater 2010;44:3133–50.
[33] Jiang B, Batra RC. Micromechanical modeling of a composite containing piezoelectric and shape memory alloy inclusions. J Intell Mater Syst 2001;12:165–82.
[34] Jiang B, Batra RC. Effective properties of a piezocomposite containing shape memory alloy and inert inclusions. Contin Mechs Thermodynam 2002;14:87–111.
[35] Jiang B, Batra RC. Effective electroelastic properties of a piezocomposite with viscoelastic and dielectric relaxing matrix. J Intell Mater Syst 2001;12:847–66.